CHEST

Thoracic Quantitative Dynamic MRI to Understand Developmental Changes in Normal Ventilatory Dynamics

Yubing Tong, PhD; Jayaram K. Udupa, PhD; Joseph M. McDonough, MS; Caiyun Wu, MS; Changjian Sun, PhD; Catherine Qiu, MS; Carina Lott, MS; Nirupa Galagedera, BA; Jason B. Anari, MD; Oscar H. Mayer, MD; Drew A. Torigian, MD; and Patrick J. Cahill, MD

BACKGROUND: A database of normative quantitative measures of regional thoracic ventilatory dynamics, which is essential to understanding better thoracic growth and function in children, does not exist.

RESEARCH QUESTION: How to quantify changes in the components of ventilatory pump dynamics during childhood via thoracic quantitative dynamic MRI (QdMRI)?

STUDY DESIGN AND METHODS: Volumetric parameters were derived via 51 dynamic MRI scans for left and right lungs, hemidiaphragms, and hemichest walls during tidal breathing. Volume-based symmetry and functional coefficients were defined to compare left and right sides and to compare contributions of the hemidiaphragms and hemichest walls with tidal volumes (TVs). Statistical analyses were performed to compare volume components among four age-based groups.

RESULTS: Right thoracic components were significantly larger than left thoracic components, with average ratios of 1.56 (95% CI, 1.41-1.70) for lung TV, 1.81 (95% CI, 1.60-2.03) for hemidiaphragm excursion TV, and 1.34 (95% CI, 1.21-1.47) for hemichest wall excursion TV. Right and left lung volumes at end-expiration showed, respectively, a 44% and 48% increase from group 2 ($8 \leq$ age < 10) to group 3 ($10 \leq$ age < 12). These numbers from group 3 to group 4 ($12 \leq$ age ≤ 14) were 24% and 28%, respectively. Right and left hemichest wall TVs exhibited, respectively, 48% and 45% increases from group 3 to group 4.

INTERPRETATION: Normal right and left ventilatory volume components have considerable asymmetry in morphologic features and dynamics and change with age. Chest wall and diaphragm contributions vary in a likewise manner. Thoracic QdMRI can provide quantitative data to characterize the regional function and growth of the thorax as it relates to ventilation.

CHEST 2021; 159(2):712-723

KEY WORDS: normal thoracic function; pulmonary function testing; quantitative dynamic MRI; thoracic insufficiency syndrome; ventilatory pump

ABBREVIATIONS: BCWtv = bilateral hemichest wall excursion tidal volume; BDtv = bilateral hemidiaphragm excursion tidal volume; BLtv = bilateral lung tidal volume; BLVee = bilateral lung volume at end-expiration; BLVei = bilateral lung volume at end-inspiration; DL = deep learning; dMRI = dynamic MRI; EE = end-expiration; EI = end-inspiration; FRC = functional residual capacity; LCWtv = left hemichest wall excursion tidal volume; LDtv = left hemidiaphragm excursion tidal volume; LLtv = left lung tidal volume; LLVee = left lung volume at end-expiration; LLVei = left lung volume at end-inspiration; PFT = pulmonary function testing; QdMRI = quantitative dynamic MRI; RCWtv = right hemichest wall excursion tidal volume; RDtv = right hemidiaphragm excursion tidal volume; RLtv = right lung tidal volume; RLVee = right lung volume at end-expiration; RLVei = right lung volume at end-inspiration; ROI = region of interest; TIS = thoracic insufficiency syndrome; TV = tidal volume

AFFILIATIONS: From the Medical Image Processing Group (Drs Tong, Udupa, Sun, and Torigian; and Ms Wu), Department of Radiology, University of Pennsylvania, and The Wyss/Campbell Center for Thoracic Insufficiency Syndrome (Mr McDonough;

The thoracic ventilatory pump accomplishes bulk transfer of air to and from the lungs. Impairments in ventilatory pump function leading to thoracic insufficiency syndrome (TIS) are the result of a complex interplay among spinal and chest wall deformity, lung parenchymal dysfunction, and neuromuscular disease. It is crucial to assess the relative volume changes of (1) left and right lungs, (2) left and right hemidiaphragms, and (3) left and right hemichest walls in a fully 4-D method, which is possible using thoracic dynamic MRI (dMRI).

TIS is a rare but serious disorder involving thoracic ventilation-loss pathologic characteristics associated with more than 27 pediatric syndromes.[1] Progressive loss of functional lung volume leads to respiratory failure and risk of early mortality in untreated TIS.[2] Currently, orthopedic treatment heavily depends on surgeon experience, and clinical outcomes for TIS treatment generally are qualitative. Quantitative assessment of regional thoracic function in TIS patients is challenging because of the lack of robust metrics for assessment of TIS, describing effects of correction, and guiding instrumentation development.[3-5]

Of concern, the ability to assess pulmonary function is limited to those patients with the cognitive and developmental capacity to follow directions and give maximum effort; however, the datum produced is a single measure with no regional differentiation of function.[6] Therefore, a dynamic imaging method that can report on regional variation of respiratory or thoracic function is needed. Additionally, a database of quantitative functional metrics describing the ventilatory pump dynamics during normal pediatric growth of the thorax does not exist. Such a normative database is vital to understand ventilatory morphologic features and function throughout childhood better.

The standard outcome measure for scoliosis-corrective surgical procedures in TIS has remained the Cobb measurement of the anteroposterior and lateral radiographic spinal curve.[7-9] However, no correlation exists between Cobb measurement and lung vital capacity,[10] limiting its value.[11] Although pulmonary function testing (PFT) indirectly can infer global respiratory function,[12] it cannot provide regional data regarding the ventilation of the individual lungs and their hemichest wall and hemidiaphragm contributions. Currently, radiography,[7-9] CT imaging,[13-15] MRI,[16,17] cine-slice MRI,[18] cine CT imaging,[19] and ultrasonography[20] are used to characterize spine and chest wall deformity. However, none of these methods can define motion deficit clearly because of thoracic impairment, and ionizing radiation exposure concerns exist regarding some of them.[21] However, thoracic dMRI[4,5,22,23] can be performed during free breathing and without breath holding, flow measurement, or external devices for respiratory gating,[24,25] which makes it extremely useful clinically. With the 4-D image derived from dMRI, we can design standard objective functional metrics that comprehensively describe the 3-D thoracic-abdominal structures and their 4-D dynamics[4,5] over growth maturation. Our goal in the current study was to quantify and describe changes in normal thoracic dynamics during childhood maturation via quantitative dynamic MRI (QdMRI) to create a normative comparison group for patients with TIS.

Methods

All data were acquired under an ongoing research protocol approved by the institutional review boards at the Children's Hospital of Philadelphia and the University of Pennsylvania, along with a Health Insurance Portability and Accountability Act waiver. We enrolled healthy children 6 to 14 years of age with the following exclusion criteria: (1) history of thoracic surgery, (2) history of asthma or other lung disease, (3) respiratory tract illness within the previous 30 days, and (4) history of scoliosis or other congenital skeletal abnormality. An image review process excluded low-quality MRI scans and images representing irregular breathing or body movement during acquisition. Thoracic dMRI scans and PFT from 51 participants (24 boys [mean age ± SD, 11.1 ± 2.4 years] and 27 girls [mean age ± SD, 10.1 ± 2.3 years]) were used in this work.

All participants were tested at the Children's Hospital of Philadelphia PFT Lab using the helium-dilution method for static lung volumes while in the supine position to mimic body position during imaging (Pneumotrac Spirometry; Morgan Scientific). The functional residual capacity (FRC) was adjusted for height-based estimated anatomic dead space resulting from nonlung airway volume not being included in the method of QdMRI.

dMRI Scan Acquisition and Construction

The thoracic dMRI protocol was performed as follows: 3-Tesla MRI scanner (Verio; Siemens); true-fast imaging with steady-state precession sequence; repetition time, 3.82 ms; echo time, 1.91 ms;

Mss Qiu, Lott, and Galagedera; and Drs Anari, Mayer, and Cahill), Children's Hospital of Philadelphia, Philadelphia, PA.

FUNDING/SUPPORT: This study was funded by the Children's Hospital of Philadelphia [Frontier Grant] and the National Institutes of Health [Grant 1R01HL150147-01].

CORRESPONDENCE TO: Jayaram K. Udupa, PhD, Medical Image Processing Group, Department of Radiology, University of Pennsylvania, 3710 Hamilton Walk, Goddard Bldg, 6th Floor, Philadelphia, PA 19104; e-mail: jay@pennmedicine.upenn.edu

DOI: https://doi.org/10.1016/j.chest.2020.07.066

voxel size, approximately 1 × 1 × 6 mm^3; 320 × 320 matrix; bandwidth, 258 Hz; and flip angle, 76°. For each sagittal location across the thorax, 80 slices were obtained over several tidal breathing cycles at approximately 200 ms/slice. On average, 35 locations across the chest were imaged. Therefore, a total of 2,800 (35 × 80) 2-D MRI slices were available to construct one representative 4-D image comprising one full breathing cycle. Patients were awake and asked to breathe naturally during scanning.

An image-based 4-D MRI construction approach[22] was used. The method performs graph-based optimization to select approximately 200 slices from among the 2,800 to form a spatiotemporal sampling of the thorax over one respiratory cycle. Previous results from a dynamic 4-D lung phantom[22] show 3% error between the image-derived volumes and the known physical volumes of the phantom for the 4-D construction method. Intensity nonuniformity correction and intensity standardization were applied to the 4-D constructed image, and previous research has shown that these operations are vital for quantitative analysis of MRI scans.[26-28]

Lung Segmentation via Deep Learning

A 2-D u-net type of deep learning (DL) network was implemented.[29,30] U-net has an encoder-decoder structure from left to right. The encoder extracts features from the image and builds a latent representation of the features suitable for the lung region by performing various convolution as well as down-sampling and max-pooling operations on the image. The decoder produces the segmentation mask by taking this representation and up-sampling the image from the previous layer (to propagate context information to higher-resolution layers) with the help of skip connections. Details of the u-net architecture are provided in e-Appendix 1 and e-Figure 1. We first specified a 2-D rectangular region of interest (ROI) around the lung region on the slice passing through the middle of the ipsilateral hemidiaphragm at end-inspiration (EI) of the 4-D image. Then, the ROI was propagated to all other slices. Segmentation then was performed automatically on all 2-D slices within the ROI.

For training and subsequent testing of the segmentation method, we used 30 of the 51 4-D data sets as follows. First, we manually segmented the 3-D lungs at their respective end-expiration (EE) and EI time points in the breathing cycle using Computer Assisted Visualization and Analysis Software System software.[31] This yielded 60 segmented 3-D images. We used 45 of these 3-D image datasets (comprising approximately 1,575 slices) for training the DL network and the remaining 15 3-D image datasets for testing. This process was repeated for 10 different combinations of training and testing dataset division. The mean and SD of the Dice coefficient[32] over the 150 tested 3-D images was 0.93 ± 0.02. We also visually compared

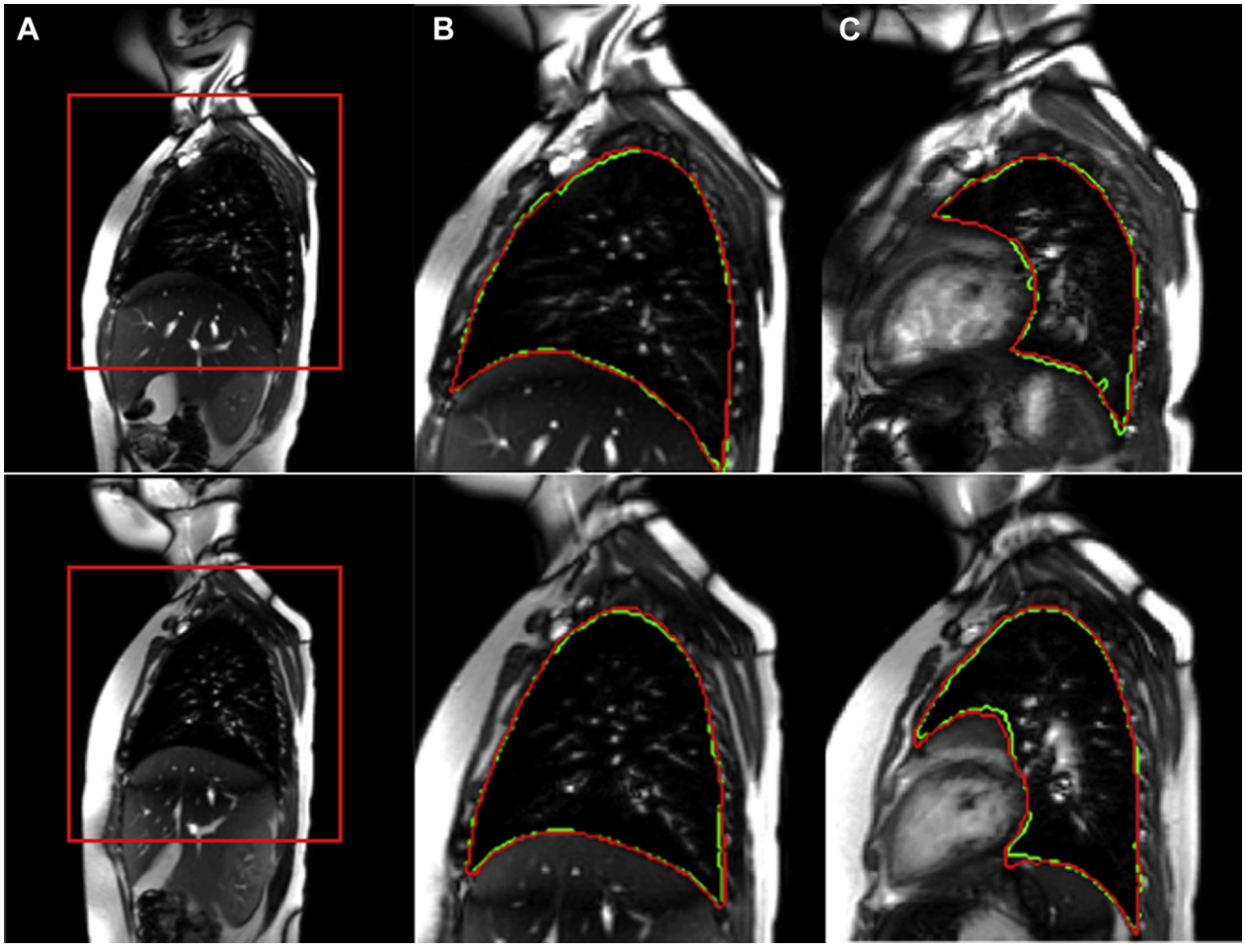

Figure 1 – *Image data for a normal 7.5-year-old male (top row) and a normal 8.2-year-old female (bottom row). A, A region of interest (ROI) placed around the right lung on a sagittal slice passing through the middle of the right hemidiaphragm at the end-inspiration (EI) time point. B, For the slice in A, corresponding ground truth manual segmentation (red) and deep learning (DL) segmentation (green) of the right lung. C, From the same image data, representative ground truth and DL segmentations for a sagittal slice passing through the left lung at the EI time point.*

automatic segmentation results with their manually segmented counterparts and found that all results were acceptable visually. Subsequently, we used the trained DL network to segment the remaining 21 4-D data sets. Figure 1 shows ROI placement and lung segmentation results from manual segmentation and DL approaches in two of the study participants.

From the 4-D image segmentations, we computed the QdMRI parameters of interest as follows.[5] The volumes of the lungs at EE and EI were computed from the segmented 3-D images. To measure the excursion from EE to EI, which is the tidal volume (TV), we first subtract the EE 3-D segmentation from the EI segmentation for each lung separately and then, in the subtracted image, separate the hemichest wall and hemidiaphragm excursion regions. For the hemichest wall component, we focused on the outer (lateral, anterior, and posterior) peripheral portions only, and not on the changes taking place from EE to EI elsewhere internally medially. For more details, please refer to Tong et al.[5] This effectively apportions the TV among the four basic anatomic displacements of the ventilatory pump, plus the remaining internal excursion regions. Figure 2 illustrates the QdMRI-derived volume components of the thoracic ventilatory pump.

QdMRI Parameters

We computed 15 QdMRI parameters as follows: right lung volume at EI (RLVei), left lung volume at EI (LLVei), bilateral (ie, combined right and left) lung volume at EI (BLVei), right lung volume at EE (RLVee), left lung volume at EE (LLVee), bilateral lung volume at EE (BLVee), right lung TV (RLtv), left lung TV (LLtv), bilateral lung TV (BLtv), right hemidiaphragm excursion TV (RDtv), left hemidiaphragm excursion TV (LDtv), bilateral hemidiaphragm excursion TV (BDtv), right hemichest wall excursion TV (RCWtv), left hemichest wall excursion TV (LCWtv), and bilateral hemichest wall excursion TV (BCWtv). The 15 parameters relate as: RLtv = RDtv + RCWtv, LLtv = LDtv + LCWtv, BLtv = LLtv + RLtv, BDtv = LDtv + RDtv, and BCWtv = LCWtv + RCWtv. For the reasons mentioned previously, RLVei - RLVee ≥ RLtv; similar inequalities hold for left lung and bilateral lung values.

To characterize further any bilateral symmetry or asymmetry in morphologic features and dynamics, we define an index of symmetry, denoted by α, for the bilateral thoracic components based on any parameters L and R relating to the left and right components, respectively, as follows:

$$\alpha = \frac{R-L}{R+L}, \text{ or } R = \left(\frac{1+\alpha}{1-\alpha}\right) \times L = r(R,L) \times L,$$
$$\text{where } r(R,L) = R/L$$

We refer to r as the symmetry coefficient. Note that in case of perfect symmetry, $R = L$, $\alpha = 0$, and $r = 1$. However, in case of asymmetry, when $R < L$, then $\alpha < 0$ and $r < 1$, and when $R > L$, then $\alpha > 0$ and $r > 1$.

To study and characterize further the functional relationship of the active chest wall and diaphragm, we define eight functional coefficients denoted $\rho(x, y) = x / y$, including: bilateral hemidiaphragm (relative to bilateral lungs), ρ(BDtv, BLtv) = BDtv / BLtv; right hemichest wall (relative to right hemidiaphragm), ρ(RCWtv, RDtv) = RCWtv / RDtv; left hemichest wall (relative to left hemidiaphragm), ρ(LCWtv, LDtv) = LCWtv / LDtv; right hemidiaphragm (relative to bilateral hemidiaphragms), ρ(RDtv, BDtv) = RDtv / BDtv; and right hemichest wall (relative to bilateral hemichest walls), ρ(RCWtv, BCWtv) = RCWtv / BCWtv. From these, other functional coefficients can be calculated as ρ(BCWtv, BLtv) = 1 - ρ(BDtv, BLtv), ρ(LDtv, BDtv) = 1 - ρ(RDtv, BDtv), and ρ(LCWtv, BCWtv) = 1 - ρ(RCWtv, BCWtv).

Statistical Analysis

Linear regression was used to illustrate the relationships between QdMRI parameters and participant age. QdMRI volume values (mean ± SD) for age-based groups were computed separately and

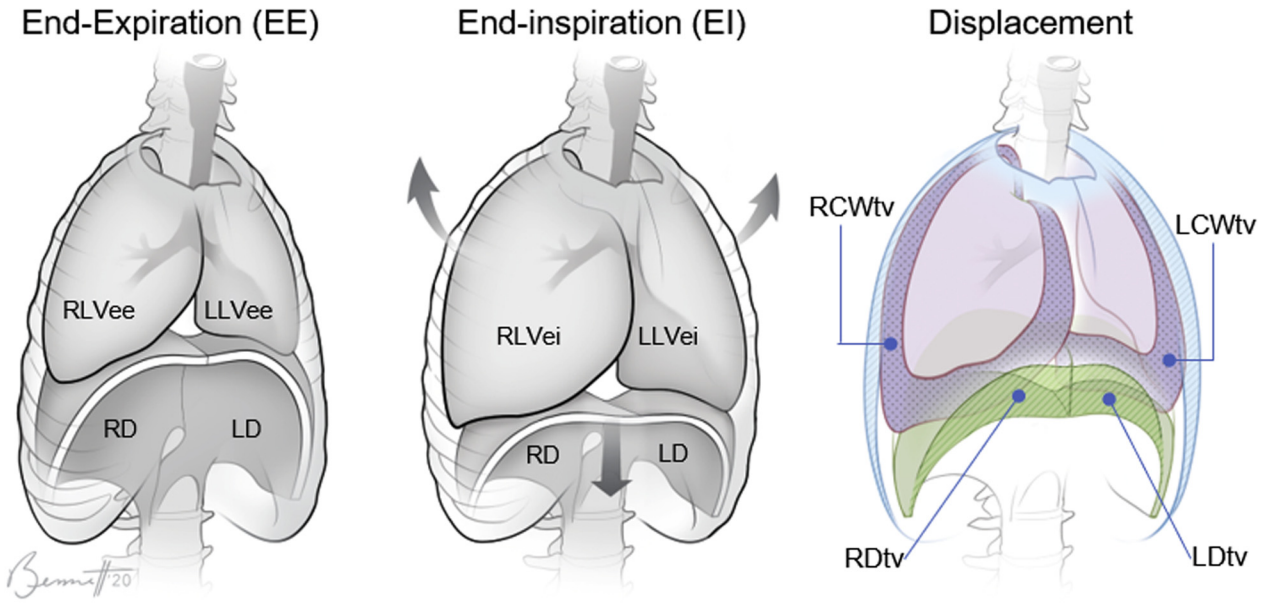

Figure 2 – *An illustration of the thoracic ventilatory pump and its volume components. Volumes of lung at EE and EI and tidal volume displacements of the chest wall and diaphragm after inspiration are depicted. EE = end-expiration; EI = end-inspiration; LCWtv = left hemichest wall excursion tidal volume; LD = left hemidiaphragm; LDtv = left hemidiaphragm excursion tidal volume; LLVee = left lung volume at end-expiration; LLVei = left lung volume at end-inspiration; RCWtv = right hemichest wall excursion tidal volume; RD = right hemidiaphragm; RDtv = right hemidiaphragm excursion tidal volume; RLVee = right lung volume at end-expiration; RLVei = right lung volume at end-inspiration.*

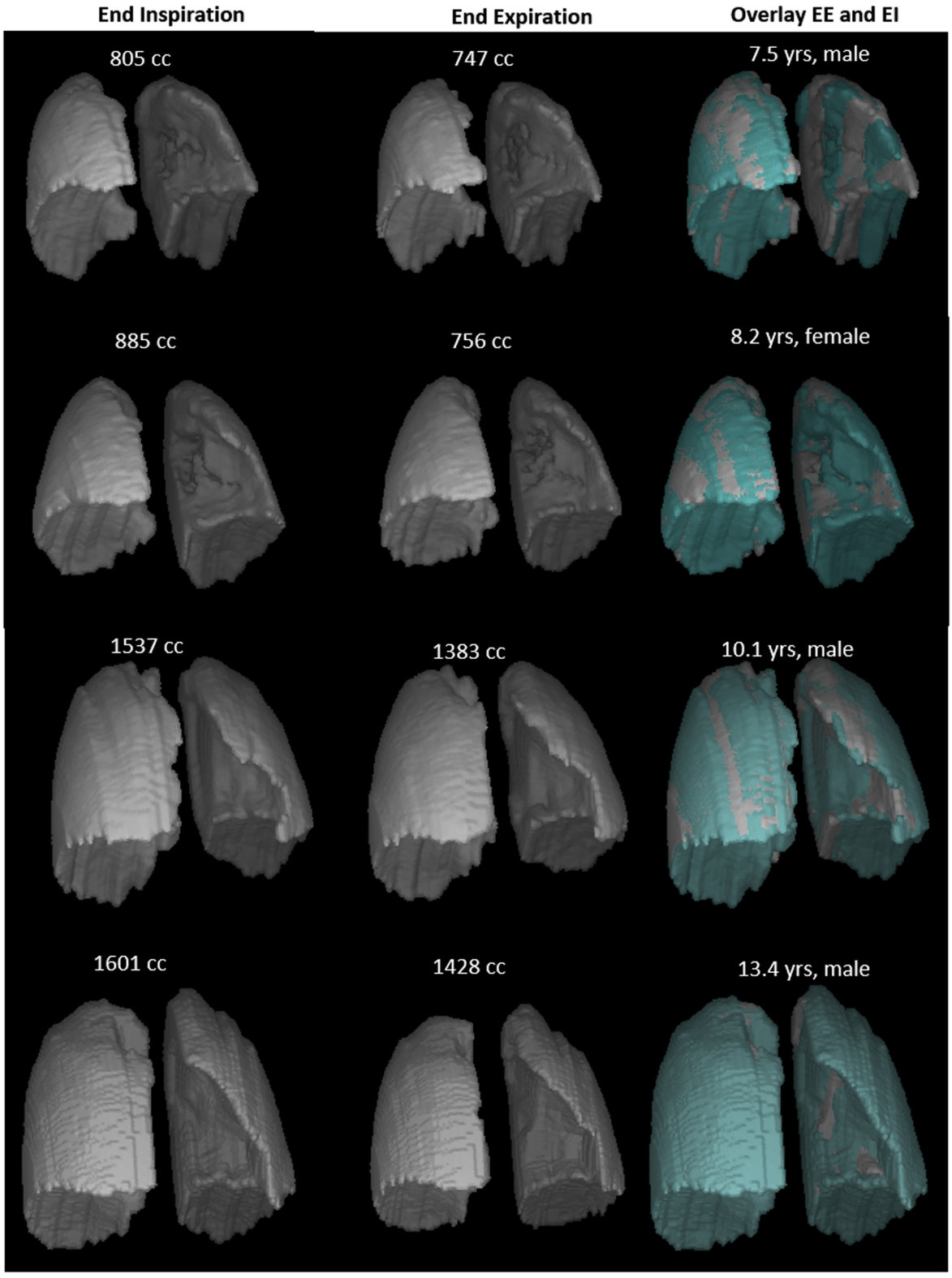

Figure 3 – *3-D lung surface renditions at end-inspiration and end-expiration generated from lung segmentations of thoracic dMRI in 4 normal children with calculated whole lung volumes (in mL). See Figure 2 legend for expansion of abbreviations.*

were compared using unpaired Student *t* tests. The paired Student *t* test was used to compare lung, hemichest wall, and hemidiaphragm volumes between left and right sides. A P value of $< .05$ was considered to indicate statistical significance. The Pearson correlation coefficient was calculated between FRC measured by PFT and the analogous QdMRI parameter BLVee.

Results

Figure 3 shows 3-D lung surface renditions at EI and EE in 4 participants. Animation of 4-D lung motion during a single breathing cycle of two children (a boy 13.4 years of age and a girl 8.2 years of age) can be found in e-Figure 2.

Figure 4 illustrates the correlation between FRC and BLVee for the age groups ($r = 0.99$). The average difference between BLVee and FRC was -2.5% (SD, 19.4%) for the entire cohort. Additionally, FRC and BLVee correlated strongly with group heights: $r = 0.99$ and $r = 0.99$, respectively.

Table 1 summarizes age, height, weight, FRC, and QdMRI volumetric data for the entire study cohort grouped into four combined-sex age range groups. As expected, overall volume averages increased with the age of the groups. Linear regression of QdMRI volumetric parameters vs age can be found in e-Figure 3. Table 2 lists the P values from t test comparisons of adjacent age-based groups. Statistically significant differences appear in boldface.

We observed that QdMRI-derived right and left lung volumes at EE (analogous to FRC) statistically significantly increased between groups 2 and 3 and between groups 3 and 4. Right and left lung TVs and hemidiaphragmatic excursion TVs did not exhibit a statistically significant difference between adjacent age groups. However, right and left hemichest wall excursion TVs did show significant increases from age groups 3 to 4.

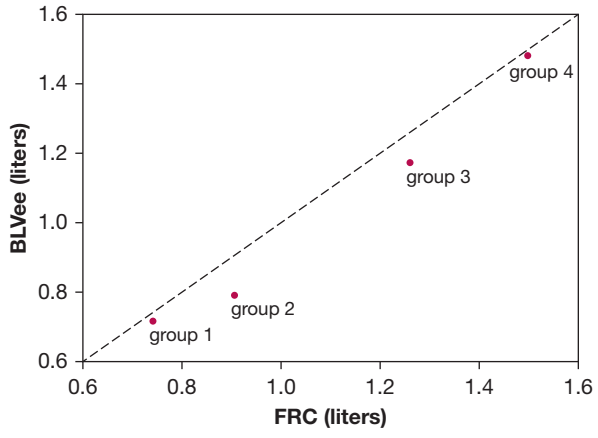

Figure 4 – *BLVee derived from quantitative dynamic MRI (QdMRI) compared to FRC measured by Helium Dilution for the four age groups. Line of equality is shown (dashed). BLVee = bilateral lung volume at end-expiration.*

Table 3 summarizes the symmetry parameters and their 95% CIs where α and r are estimated over all participants. We observed that all right lung components among the QdMRI parameters were statistically significantly larger than left lung components ($P < .0001$), and as such that $\alpha > 0$ and $r > 1$. Therefore, r indicates how much larger the right component is relative to the left component. For example, on average, RDtv is 81% larger than LDtv.

Table 4 summarizes the functional coefficients and their 95% CIs using all participants. Overall, on average, for the thoracic ventilatory pump at supine rest, 56% of the TV is attributable to diaphragmatic excursion and the remainder is the result of chest wall excursion. Considering the total diaphragm, the right hemidiaphragm provides 62% of its total excursion for TV, with the balance on the left. Considering the chest wall alone, the right hemichest wall provides 56% of its total excursion for TV, with the balance on the left. The right hemichest wall excursion is smaller than that of the right hemidiaphragm (83%), whereas the left hemichest wall excursion is slightly larger than that of the left hemidiaphragm (103%).

Discussion

At present, a normative database of quantitative metrics describing regional morphologic features, dynamics, growth, symmetry, and function of the thoracic components during childhood maturation does not exist. Such data are vital to understand what is "normal" in children as they grow and to perform knowledge-based TIS assessment, surgical planning, and postoperative outcome evaluation by comparing nearness with normality. In this study, we applied QdMRI to 51 normal pediatric thoracic dMRI datasets and investigated volumetric thoracic QdMRI parameters and their changes with growth. To our knowledge, these or similar parameters describing the morphologic features and dynamics of the separate thoracic ventilatory pump components have not been reported in any previous research.

TABLE 1] Age, Height, Weight, Functional Residual Capacity, and QdMRI Parameters for the Study Cohort

Parameter	Abbreviation	Group 1	Group 2	Group 3	Group 4	All
Age, y		6.9 (0.5)	8.9 (0.5)	11.2 (0.6)	13.0 (0.6)	10.59 (2.3)
Height, cm		122.8 (7.5)	132.8 (5.0)	147.2 (8.8)	161.7 (9.5)	144.69 (16.9)
Weight, kg		27.0 (7.4)	29.9 (5.3)	43.9 (14.4)	50.5 (13.8)	40.30 (15.06)
Functional residual capacity, mL	FRC	976.0 (184.9)	1,176.7 (315.4)	1,616.7 (460.8)	1,881.2 (451.0)	1,501.6 (523.2)
Right lung volume at end-inspiration, mL	RLVei	448.5 (76.8)	501.4 (107.5)	724.7 (142.6)	901.8 (187.1)	690.2 (231.3)
Left lung volume at end-inspiration, mL	LLVei	338.3 (52.3)	370.1 (114.4)	549.4 (116.0)	703.8 (184.0)	527.8 (198.8)
Bilateral lung volume at end-inspiration, mL	BLVei	786.8 (122.9)	871.5 (220.5)	1,274.1 (244.4)	1,605.5 (360.3)	1,218.0 (423.7)
Right lung volume at end-expiration, mL	RLVee	407.0 (64.1)	457.8 (87.7)	667.3 (134.7)	830.9 (194.2)	633.8 (220.3)
Left lung volume at end-expiration, mL	LLVee	306.7 (49.5)	330.4 (93.9)	503.7 (115.1)	647.9 (176.1)	482.6 (187.8)
Bilateral lung volume at end-expiration, mL	BLVee	713.7 (110.5)	788.2 (179.6)	1,171.1 (234.8)	1,478.8 (363.0)	1,116.4 (402.9)
Right lung tidal volume, mL	RLtv	44.6 (13.8)	51.9 (24.7)	70.7 (27.9)	88.1 (22.8)	68.1 (28.5)
Left lung tidal volume, mL	LLtv	31.3 (8.7)	38.6 (20.6)	48.9 (20.1)	56.8 (17.7)	46.3 (19.7)
Bilateral lung tidal volume, mL	BLtv	75.9 (19.2)	90.5 (42.6)	119.6 (42.2)	144.9 (33.3)	114.3 (44.0)
Right hemidiaphragm excursion tidal volume, mL	RDtv	22.8 (5.9)	32.2 (18.0)	45.4 (23.1)	50.7 (17.9)	40.4 (20.7)
Left hemidiaphragm excursion tidal volume, mL	LDtv	16.7 (5.6)	20.6 (12.4)	28.1 (18.0)	27.2 (9.6)	24.2 (13.1)
Bilateral hemidiaphragm excursion tidal volume, mL	BDtv	39.5 (9.7)	52.7 (27.7)	73.5 (34.8)	77.8 (23.7)	64.6 (29.9)
Right hemichest wall excursion tidal volume, mL	RCWtv	19.7 (9.2)	21.8 (9.9)	25.4 (9.0)	37.4 (12.8)	27.7 (12.6)
Left hemichest wall excursion tidal volume, mL	LCWtv	14.6 (4.0)	18.0 (10.2)	20.8 (7.4)	29.7 (12.5)	22.0 (10.9)
Bilateral hemichest wall excursion tidal volume, mL	BCWtv	36.4 (12.4)	37.7 (18.9)	46.1 (14.6)	67.1 (23.9)	49.7 (22.2)

Data are presented as mean (SD). Group 1, $6 \leq$ age < 8 (n = 10); group 2, $8 \leq$ age < 10 (n = 9); group 3, $10 \leq$ age < 12 (n = 15); group 4, $12 \leq$ age ≤ 14 (n = 17). QdMRI = quantitative dynamic MRI.

TABLE 2] *P* Values From Student *t* Tests on Parameters for Age-Based Groups for the Study Cohort

Parameter	Abbreviation	Group 1 vs Group 2	Group 2 vs Group 3	Group 3 vs Group 4
Age, y	…	**< .0001**	**< .0001**	**< .0001**
Height, cm	…	**.001**	**< .0001**	**< .0001**
Weight, kg	…	.17	**.002**	.09
Functional residual capacity, mL	FRC	.07	**.007**	**.045**
Right lung volume at end-inspiration, mL	RLVei	.24	**.0003**	**.005**
Left lung volume at end-inspiration, mL	LLVei	.46	**.002**	**.008**
Bilateral lung volume at end-inspiration, mL	BLVei	.17	**.0001**	**.009**
Right lung volume at end-expiration, mL	RLVee	.17	**.0001**	**.009**
Left lung volume at end-expiration, mL	LLVee	.51	.0007	.01
Bilateral lung volume at end-expiration, mL	BLVee	.30	.0002	.008
Right lung tidal volume, mL	RLtv	.50	.10	.07
Left lung tidal volume, mL	LLtv	.35	.25	.07
Bilateral lung tidal volume, mL	BLtv	.37	.12	.07
Right hemidiaphragm excursion tidal volume, mL	RDtv	.17	.13	.48
Left hemidiaphragm excursion tidal volume, mL	LDtv	.41	.24	.86
Bilateral hemidiaphragm excursion tidal volume, mL	BDtv	.21	.12	.69
Right hemichest wall excursion tidal volume, mL	RCWtv	.64	.16	**.004**
Left hemichest wall excursion tidal volume, mL	LCWtv	.37	.49	**.02**
Bilateral hemi-chest wall excursion tidal volume, mL	BCWtv	.86	.27	**.005**

Group 1, 6 ≤ age < 8 (n = 10); group 2, 8 ≤ age < 10 (n = 9); group 3, 10 ≤ age < 12 (n = 15); and group 4, 12 ≤ age ≤ 14 (n = 17). *P* values < .05 appear in boldface.

Establishing the comparableness and relative accuracy of our QdMRI method for this study, we found that QdMRI-derived bilateral lung volume measurements at EE were approximately equal to and showed high correlation with FRC measured by PFT, given that the two methods measure the lung at the same point in the breathing cycle while patients are in the supine position and relaxed.

Height is known to be the strongest correlate with lung volume. The height difference between boys and girls in our age groups 1, 2, and 3 was not significant. Only in group 4 (12-14 years of age) were boys observed to be significantly taller than girls ($P = .04$), which accords with height difference between boys and girls becoming distinct at puberty. Therefore, the effects of sex and height were not considered in this study, and age was used instead as the grouping criterion. Furthermore, age rather than height may be expected to reflect better differences in morphologic maturity related to the skeleton and thoracic ventilatory pump structure. All average QdMRI parameters and FRC show increase with age, as expected, among the age-based groups, as shown

TABLE 3] Index of Symmetry α and Symmetry Coefficient *r* for QdMRI Parameters for the Study Cohort

α	α(RLVei, LLVei)	α(RLVee, LLVee)	α(RLtv, LLtv)	α(RDtv, LDtv)	α(RCWtv, LCWtv)
Mean ± SD	0.14 ± 0.06	0.14 ± 0.05	0.19 ± 0.16	0.23 ± 0.21	0.11 ± 0.16
95% CI	0.12-0.15	0.13-0.16	0.14-0.23	0.18-0.29	0.07-0.16
R	*r*(RLVei, LLVei)	*r*(RLVee, LLVee)	*r*(RLtv, LLtv)	*r*(RDtv, LDtv)	*r*(RCWtv, LCWtv)
Mean ± SD	1.33 ± 0.16	1.34 ± 0.14	1.56 ± 0.54	1.81 ± 0.78	1.34 ± 0.49
95% CI	1.29-1.38	1.30-1.38	1.41-1.70	1.60-2.03	1.21-1.47
P value (right, left)	< .0001	< .0001	< .0001	< .0001	< .0001

LCWtv = left hemichest wall excursion tidal volume; LDtv = left hemidiaphragm excursion tidal volume; LLtv = left lung tidal volume; LLVee = left lung volume at end-expiration; LLVei = left lung volume at end-inspiration; RCWtv = right hemichest wall excursion tidal volume; RDtv = right hemidiaphragm excursion tidal volume; RLtv = right lung tidal volume; RLVee = right lung volume at end-expiration; RLVei = right lung volume at end-inspiration. See Table 1 legend for expansion of other abbreviations.

TABLE 4] Functional Coefficient (ρ) for QdMRI Parameters for the Study Cohort

QdMRI Parameter	Mean (SD)	95% CI
Bilateral diaphragm, ρ(BDtv, BLtv)	0.56 (0.10)	0.53-0.59
Bilateral chest wall, ρ(BCWtv, BLtv)	0.44 (0.10)	0.41-0.47
Right hemidiaphragm, ρ(RDtv, BDtv)	0.62 (0.11)	0.59-0.65
Left hemidiaphragm, ρ(LDtv, BDtv)	0.38 (0.11)	0.35-0.41
Right chest wall, ρ(RCWtv, BCWtv)	0.56 (0.08)	0.54-0.58
Left chest wall, ρ(LCWtv, BCWtv)	0.44 (0.08)	0.42-0.46
Right chest wall to hemidiaphragm, ρ(RCWtv, RDtv)	0.83 (0.57)	0.67-0.98
Left chest wall to hemidiaphragm, ρ(LCWtv, LDtv)	1.03 (0.45)	0.90-1.15

BDtv = bilateral hemidiaphragm excursion tidal volume; BCWtv = bilateral hemichest wall excursion tidal volume. See Table 1 and 3 legends for expansion of other abbreviations.

in Table 1. Table 2 shows that significant changes with age were observed between groups 2 and 3 and between groups 3 and 4 for RLVee and LLVee, as well as for RCWtv and LCWtv. These changes in the chest wall contribution to TV may reflect rib cage development during early puberty.

We defined symmetry parameters to assess right to left differences in lung volume and ventilatory pump components. We found that in healthy children, left and right thoracic components (especially TVs) are not symmetric, because right thoracic component volumes are significantly greater than the corresponding left thoracic components. For example, we observed average volume ratios of 1.56 (95% CI, 1.41-1.70) for right lung TV relative to left lung TV, 1.81 (95% CI, 1.60-2.03) for the right hemidiaphragm contribution relative to that of the left hemidiaphragm, and 1.34 (95% CI, 1.21-1.47) for the right hemichest wall contribution relative to that of the left hemichest wall. Because we did not have a sufficiently large sample size, we did not assess symmetry parameters by age group or how they may change with growth. A previous study showed that ventilation scans in heathy older children and adults ascribed 55% of function to the right

Figure 5 – *Radiograph images for a 11-year-old male Myelomeningocele patient before (left) and after surgery (right) involving implant of bilateral growth-sparing devices to straighten/stabilize the spine and limit loss of thoracic volume.*

TABLE 5] Index of Symmetry α and Functional Coefficient (ρ) for Patient Example

Parameter	Before Surgery	After Surgery	Normal Value	Absolute Value	
				Difference Before	Difference After
α(RLtv, LLtv)	−0.43	0.38	0.19	0.62	0.19
α(RDtv, LDtv)	−0.29	0.43	0.23	0.52	0.20
α(RCWtv, LCWtv)	−0.49	0.29	0.11	0.60	0.18
ρ(RCWtv, RDtv)	1.50	0.41	0.83	0.67	0.42
ρ(LCWtv, LDtv)	2.43	0.56	1.03	1.40	0.47

See Table 3 legend for expansion of abbreviations.

lung and 45% of function to the left lung.[33] Lung function of the right and left components was not symmetric, which is consistent with our results.

It can be determined from our data in Tables 1 and 3 that, on average for the cohort, the TV of healthy participants was supplied by 35% from the right hemidiaphragm, 21.5% from the left hemidiaphragm, 24% from the right hemichest wall, and 19.5% from the left hemichest wall. The right hemidiaphragm was the primary contributor to TV in the healthy participants. This type of information is important for assessing patients with disorders such as TIS, planning corrective surgical operations, and assessing outcomes.

Other insightful interpretations of the QdMRI volumetric data are possible. For example, in the healthy participants, the index of symmetry parameters α(RLVee, LLVee) and α(RLVei, LLVei) remained equal during the tidal breath (close to a value of 1.33). In the case of unilateral thoracic restriction, it is likely that these values would be different from normal and would not be equal at EI.

An example of using the thoracic QdMRI parameters for presurgical and postsurgical evaluation of a TIS patient is shown in Figure 5 and Table 5. After implant of instrumentation, it can be seen that the volumetric relationship between right and left TV components, as indicated by the index of symmetry α, moves closer to the expected normal values. Also, the relationship between unilateral chest wall and diaphragm contribution to TV, as indicated by the functional coefficient ρ, also moves closer to expected normal values. We currently are devising mathematical methods to incorporate various groups of the thoracic symmetry and function parameters, along with percent predicted volumes, into clinically quantitative and qualitative expressions to determine changes after surgery for TIS.[32]

Few publications have investigated thoracic childhood maturation based on medical images. One somewhat related article[34] used nondynamic CT imaging datasets from children and adults for determining age-related changes in thoracic structure where lung volumes derived from CT scanning and their changes with age were analyzed. One conclusion is that the mean lung volumes increased significantly with age in pediatric participants, which agrees with our conclusion regarding the whole lung volume change with age.[35] Our study used thoracic dMRI instead of CT scanning and extended the scope to study the regional dynamics of the thoracic components separately for both left and right sides.

The main limitation of this study is the small sample size, which prevented us from performing analyses based on more finely divided age groups of children and separately for the two sexes. Yet, we were able to demonstrate age-related differences in normal thoracic function. Another potential limitation is that thoracic dMRI scanning and data acquisition required about 40 minutes per participant, which would be challenging in clinical practice. The subsequent processing of the MRI scans to derive QdMRI parameters is not automated fully at present, and consequently requires considerable human interaction. We currently are researching and developing methods to reduce the image acquisition time significantly and to automate all image processing and analysis steps fully. We have not distinguished further the movement of different portions of the diaphragm and chest wall in this article. However, it is feasible to divide the diaphragm region uniformly into smaller regions and then to quantify and compare the movement in each subregion as well as the changes with age. This is one of our ongoing research studies.

To our knowledge, this is the first study to provide a quantitative dynamic functional method to assess

regional ventilatory pump function in healthy children and furthermore to derive indexes for right and left symmetry and right and left hemichest wall and hemidiaphragm excursion contributions. We showed how lung, hemidiaphragm, and hemichest wall excursion TVs change with age, along with the normal asymmetry of the right and left thoracic components. The presented data and methods may provide surgeons with a potential benchmark metric for quantifying outcomes in surgery for conditions such as TIS, early onset scoliosis, adolescent idiopathic scoliosis, or even adult scoliosis or kyphosis. It will enable new opportunities to understand better TIS and many other conditions that affect thoracic function, as well as the effects of therapeutic interventions, in children as well as in adults.

Acknowledgments

Author contributions: J. K. U. is the guarantor of the content of the manuscript, including the data and analysis. J. K. U. conceived the work; J. K. U., Y. T., J. M. M., D. A. T., and P. J. C. designed the work; P. J. C., J. M. M., Y. T., C. L., C Q., and N. G. acquired the data; Y. T., J. K. U., J. M. M., D. A. T., P. J. C., J. A., O. H. M., C. J. S., and C. W. analyzed and interpreted the data; Y. T. drafted the manuscript; J. K. U., D. A. T., J. M. M., P. J. C., J. A., and O. H. M. revised the manuscript critically; all authors gave final approval of the manuscript; and all authors ensured that questions related to the accuracy or integrity of any part of the work were investigated appropriately and resolved.

Financial/nonfinancial disclosures: D. A. T. and J. K. U. are co-founders of Quantitative Radiology Solutions. None declared (Y. T., J. M., C. W., C. S., C. Q., C. L., N. G., J. A., O. M., P. C.).

Role of sponsors: The sponsor had no role in the design of the study, the collection and analysis of the data, or the preparation of the manuscript.

Other contributions: The authors thank Mr Dewey Odhner for help with use of the CAVASS software system.

Additional information: The e-Appendix and e-Figures can be found in the Supplemental Materials section of the online article.

References

1. Campbell RM Jr, Smith MD. Thoracic insufficiency syndrome and exotic scoliosis. *J Bone Joint Surg Am*. 2007;89(suppl 1):108-122.
2. Corona J, Matsumoto H, Roye DP, et al. Measuring quality of life in children with early onset scoliosis: development and initial validation of the early onset scoliosis questionnaire. *J Pediatr Orthop*. 2011;31(2):180-185.
3. Nossov SB, Curatolo E, Campbell RM, et al. VEPTR: are we reducing respiratory assistance requirements? *J Pediatr Orthop*. 2019;39(1):28-32.
4. Udupa JK, Tong Y, Capraro A, et al. Understanding respiratory restrictions as a function of the scoliotic spinal curve in thoracic insufficiency syndrome: a 4D dynamic MR imaging study. *J Pediatr Orthop*. 2018;10:15-20.
5. Tong Y, Udupa JK, McDonough JM, et al. Quantitative dynamic thoracic MRI: application to thoracic insufficiency syndrome in pediatric patients. *Radiology*. 2019;292:206-213.
6. Beydon N, Davis SD, Lombardi E, et al. American Thoracic Society/European Respiratory Society Working Group on Infant and Young Children Pulmonary Function Testing. An official American Thoracic Society/European Respiratory Society statement: pulmonary function testing in preschool children. *Am J Respir Crit Care Med*. 2007;175:1304-1345.
7. Sankar WN, Albrektson J, Lerman L, et al. Scoliosis in-brace curve correction and patient preference of CAD/CAM versus plaster molded TLSOs. *J Child Orthop*. 2007;1(6):345-349.
8. Glotzbecker MP, Gold M, Puder M, et al. Scoliosis after chest wall resection. *J Child Orthop*. 2013;7:301-307.
9. Gantner AS, Braunschweig L, Tsaknakis K, et al. Spinal deformity changes in children with long-term vertical expandable prosthetic titanium rib treatment. *Spine J*. 2018;18:567-574.
10. Mayer OH, Redding G. Early changes in pulmonary function after vertical expandable prosthetic titanium rib insertion in children with thoracic insufficiency syndrome. *J Pediatr Orthop*. 2009;29:35-38.
11. Goldberg CJ, Gillic I, Connaughton O, et al. Respiratory function and cosmesis at maturity in infantile-onset scoliosis. *Spine*. 2003;28(20):2397-2406.
12. Motoyama EK, Deeney VF, Fine GF, et al. Effects on lung function of multiple expansion thoracoplasty in children with thoracic insufficiency syndrome: a longitudinal study. *Spine*. 2006;31(3):284-290.
13. Izatt MT, Adam CJ, Verzin EJ, et al. CT and radiographic analysis of sagittal profile changes following thoracoscopic anterior scoliosis surgery. *Scoliosis*. 2012;7:15.
14. Adam CJ, Cargill SC, Askin GN. Computed tomography-based volumetric reconstruction of the pulmonary system in scoliosis: trends in lung volume and lung volume asymmetry with spinal curve severity. *J Pediatr Orthop*. 2007;27(6):677-681.
15. Abul-Kasim K, Karlsson MK, Hasserius R, et al. Measurement of vertebral rotation in adolescent idiopathic scoliosis with low-dose CT in prone position—method description and reliability analysis. *Scoliosis*. 2010;5(4):1-8.
16. Chu WCW, Li AM, Ng BKW, et al. Dynamic magnetic resonance imaging in assessing lung volumes, chest wall, and diaphragm motions in adolescent idiopathic scoliosis versus normal controls. *Spine*. 2006;31(19):2243-2249.
17. Kotani T, Minami S, Takahashi K, et al. An analysis of chest wall and diaphragm motions in patients with idiopathic scoliosis using dynamic breathing MRI. *Spine*. 2004;29(3):298-302.
18. Chu WCW, Ng BKW, Li AM, et al. Dynamic magnetic resonance imaging in assessing lung function in adolescent idiopathic scoliosis: a pilot study of before and after posterior spinal fusion. *J Orthop Surg Res*. 2007;2-20:1-7.
19. Yang O, Lu W, Low DA, et al. 4D-CT motion estimation using deformable image registration and respiration motion modeling. *Med Phys*. 2008;35(10):4577-4590.
20. Chen W, Lou EH, Zhang PQ, et al. Reliability of assessing the coronal curvature of children with scoliosis by using ultrasound images. *J Child Orthop*. 2013;7(6):521-529.
21. Low DA, Nystrom M, Kalinin E, et al. A method for the reconstruction of four-dimensional synchronized CT scans acquired during free breathing. *Med Phys*. 2003;30(6):1254-1263.
22. Tong YB, Udupa JK, Ciesielski KC, et al. Retrospective 4D MR image construction from free-breathing slice acquisitions: a novel graph-based approach. *Med Image Anal*. 2017;35:345-359.
23. Wachinger C, Yigitsoy M, Rijkhorst EJ, et al. Manifold learning for image-based breathing gating in ultrasound and MRI. *Med Image Anal*. 2012;16(4):806-818.
24. Cai J, Chang Z, Wang Z, et al. Four-dimensional magnetic resonance imaging (4D-MRI) using image-based respiratory surrogate: a feasibility study. *Med Phys*. 2011;38(12):6384-6394.
25. Wagshul ME, Sin S, Lipton ML, et al. Novel retrospective, respiratory-gating method enables 3D, high resolution, dynamic imaging of the upper airway during tidal breathing. *Magn Reson Med*. 2013;70(6):1580-1590.
26. Zhuge Y, Udupa JK, Liu J, et al. Image background inhomogeneity correction in

MRI via intensity standardization. *Comput Med Imaging Graph*. 2009;33(1):7-16.

27. Nyul LG, Udupa JK. On standardizing the MR image intensity scale. *Magn Reson Med*. 1999;42(6):1072-1081.

28. Jagadale BN, Udupa JJ, Tong Y, et al. Lung parenchymal analysis on dynamic MRI in thoracic insufficiency syndrome to assess changes following surgical intervention. *Proc SPIE Int Soc Opt Eng*. 2018;10575:105753M.

29. LeCun Y, Bengio Y, Hinton G. Deep learning. *Nature*. 2015;521(7553):436-444.

30. Ronneberger O, Fisher P, Brox T. U-net: convolutional networks for biomedical image segmentation. Conference on Computer Vision and Pattern Recognition, May 18, 2015. https://arxiv.org/pdf/1505.04597.pdf. Accessed September 16, 2020.

31. Grevera G, Udupa J, Odhner D, et al. CAVASS: a computer-assisted visualization and analysis software system. *J Digit Imaging*. 2007;20(suppl 1):101-118.

32. Zou KH, Warfield SK, Bharatha A, et al. Statistical validation of image segmentation quality based on a spatial overlap index. *Acad Radiol*. 2004;11(2):178-189.

33. Redding G, Song K, Inscore S, et al. Lung function asymmetry in children with congenital and infantile scoliosis. *Spine J*. 2008;8(4):639-644.

34. Tong Y, Udupa J, McDonough J, et al. Quantitative dynamic thoracic MRI (QdMRI) on normal children and pediatric patients with Thoracic Insufficiency Syndrome (TIS): quantitative evaluation of vertical expandable prosthetic titanium rib (VEPTR)-based surgery. In: Proceedings of the Radiological Society of North America; December 1-6, 2019; Chicago, IL.

35. Well DS, Meier JM, Mahne A, et al. Detection of age-related changes in thoracic structure and function by computed tomography, magnetic resonance imaging, and positron emission tomography. *Semin Nucl Med*. 2007;37(2):103-119.